Journal of Pathology Informatics 15 (2024) 100352

Contents lists available at ScienceDirect

Journal of Pathology Informatics

journal homepage: www.elsevier.com/locate/jpi

Digital analysis of the prostate tumor microenvironment with high-order chromogenic multiplexing

Rahul Rajendran, Rachel C. Beck, Morteza M. Waskasi, Brian D. Kelly, Daniel R. Bauer *

Roche Diagnostics Solutions, (Ventana Medical Systems, Inc.), Tucson, AZ, USA

ARTICLE INFO

Keywords:
Artificial intelligence
Tumor immune microenvironment
Imaging
Spectroscopy
Phenotyping
Immunotherapy
Immunofluorescence
Umap
Immunohistochemistry
Cancer

ABSTRACT

As our understanding of the tumor microenvironment grows, the pathology field is increasingly utilizing multianalyte diagnostic assays to understand important characteristics of tumor growth. In clinical settings, brightfield chromogenic assays represent the gold-standard and have developed significant trust as the first-line diagnostic method. However, conventional brightfield tests have been limited to low-order assays that are visually interrogated. We have developed a hybrid method of brightfield chromogenic multiplexing that overcomes these limitations and enables high-order multiplex assays. However, how compatible high-order brightfield multiplexed images are with advanced analytical algorithms has not been extensively evaluated. In the present study, we address this gap by developing a novel 6-marker prostate cancer assay that targets diverse aspects of the tumor microenvironment such as prostate-specific biomarkers (PSMA and p504s), immune biomarkers (CD8 and PD-L1), a prognostic biomarker (Ki-67), as well as an adjunctive diagnostic biomarker (basal cell cocktail) and apply the assay to 143 differentially graded adenocarcinoma prostate tissues. The tissues were then imaged on our spectroscopic multiplexing imaging platform and mined for proteomic and spatial features that were correlated with cancer presence and disease grade. Extracted features were used to train a UMAP model that differentiated healthy from cancerous tissue with an accuracy of 89% and identified clusters of cells based on cancer grade. For spatial analysis, cell-to-cell distances were calculated for all biomarkers and differences between healthy and adenocarcinoma tissues were studied. We report that p504s positive cells were at least 2× closer to cells expressing PD-L1, CD8, Ki-67, and basal cell in adenocarcinoma tissues relative to the healthy control tissues. These findings offer a powerful insight to understand the fingerprint of the prostate tumor microenvironment and indicate that high-order chromogenic multiplexing is compatible with digital analysis. Thus, the presented chromogenic multiplexing system combines the clinical applicability of brightfield assays with the emerging diagnostic power of high-order multiplexing in a digital pathology friendly format that is well-suited for translational studies to better understand mechanisms of tumor development and growth.

Introduction

Brightfield histological assays are the clinical standard for cancer diagnostics and have long been the first-line method for interpreting solid tumors.[1,2] Chromogenic stains such as hematoxylin and eosin (H&E) and diaminobenzidine (DAB) are established gold-standard techniques that have become mainstays in the workflow of clinical cancer diagnostics.[3] Accordingly, brightfield assays have developed a great deal of trust in the field and they remain the assay of choice in clinical settings.[2] Although pathology laboratories continue to adopt digital tools, clinical diagnosis of primary tumors is largely performed by visual interrogation of chromogenically stained tissue such as H&E, single biomarker immunohistochemistry (IHC) staining with DAB, and special stains.[4] However, as our understanding of the complexity of tumor development and the associated immune response grows, the field is looking to multianalyte assays to reveal mechanistic drivers of tumor growth to help inform treatment decisions.[5,6] Multiplex IHC allows for the simultaneous detection of multiple biomarkers in a single tissue section and permits direct observation of different cell populations within a specimen. Multiplex IHC is therefore well-suited to help evaluate prognostic characteristics of tumor growth by detecting functionally active phenotypes as well as spatial descriptors of the disease and associated immune response.[7–10] In fact, multiplex IHC has been reported to outperform single IHC, tumor mutation burden, and gene expression profile assays in predicting response to PD-1/PD-L1 checkpoint blockade.[11]

There has recently been an explosion of digital pathology tools that can be used to quantitatively analyze histologically stained slides and extract important prognostic and predictive contextual features.[12–14] These approaches enable mining of phenotypic cellular subtypes within the spatial context of the tumor microenvironment (TME) for correlation with outcome data.[15] Features such as proximity to other cell types and distance

* Corresponding author.
E-mail address: daniel.bauer.db2@roche.com (D.R. Bauer).

http://dx.doi.org/10.1016/j.jpi.2023.100352
Received 18 July 2023; Received in revised form 30 September 2023; Accepted 16 November 2023
Available online 21 November 2023

to the tumor margin are increasingly being recognized as important to understand how the TME is functioning and what treatment options are expected to be the most beneficial.[16,17] For instance, the spatial distribution of CD8 T cells and FoxP3 tumor infiltrating lymphocytes impacts prognosis in gastric cancer.[18]

Simultaneous use of multiple conventional chromogens (DAB, Hematoxylin, Fast red) presents technical challenges to multiplex assays because the dyes have broad and overlapping absorption spectra. This makes it difficult for a pathologist to visually interrogate the tissue, especially in complicated situations such as with co-localized antigens. From an imaging perspective, conventional dyes are difficult to reliably separate which ultimately limits the capability and robustness of downstream analysis algorithms. To circumvent these technical limitations, there has been significant work developing multiplex immunofluorescence (mIF)-based approaches that have the ability to resolve colocalized antigens with high sensitivity.[19] Despite its technical performance, clinical adoption of mIF has not materialized due to the technology's high cost, low sample throughput, difficulties standardizing the system, and because clinical workflows are designed for brightfield assays.[20,21]

As previously described, we have developed a hybrid method of multiplexing that supports high-order multiplex assays.[22–24] We utilize chromogens that are conjugated with tyramide and quinone methide precursors that are enzymatically activated to covalently bind the dyes to tissue components in near proximity to the targeted protein.[22] This approach permits rapid development of new chromogens with narrowband absorption profiles and peaks tuned to be appropriately separated, so they are amenable to high-order multiplexing. The associated imaging system utilizes a purpose-built spectroscopic imaging platform and accompanying spectral deconvolution algorithms to reliably separate dyes from a stained tissue section into well-resolved images of the individual biomarkers.[23]

Brightfield multiplexing has been traditionally limited to single or low-order biomarker assays that can be readily assessed by a pathologist, although there has been increased interest recently in extending the capabilities of chromogenic multiplexing.[25,26] However, there is a shortage of work exploring how compatible high-order brightfield multiplex images are with modern digital analytical algorithms. This work addresses this gap by exploring how suitable our chromogenic multiplexing system is with modern digital pathology tools such as cell segmentation and enumeration, digital phenotyping, dimensionality reduction, and spatial biology-based algorithms.

To detail the system's capabilities, we developed a 6-marker assay (basal cell cocktail, CD8, Ki-67, p504s, PD-L1, and PSMA) using novel narrowband chromogens and imaged the assay using our spectroscopic imaging platform. This multiplex assay targets biomarkers that are recognized to be actively modulated in prostate cancer (PCa) development and progression. Basal cell expression in the human prostate is associated with normal organ development and function, which indicates that its complete absence is usually associated with malignancy.[27,28] CD8 is a marker for the population of cytotoxic T cells which are powerful effectors in the anticancer immune response and play an important role in the success of current immunotherapies.[29] CD8 helps in predicting patient survival rates as higher density of CD8 positive cells is associated with prolonged survival of high-risk PCa patients.[30] PSMA staining helps differentiate PCa risk, because 80% of patients diagnosed with PCa were PSMA positive and a higher density of PSMA in prostate glands is correlated with reduced outcomes.[31–33] p504s is a cytoplasmic protein that is highly sensitive and specific to prostate carcinoma that is absent or weakly present in benign prostate glands.[34] Furthermore, it has been reported that the combination of PSMA and p504s is advantageous for PCa detection.[35] Ki-67 is a protein that is expressed in proliferating cells in all non-rest cell cycle phases.[36] High Ki-67 proliferation index can indicate a fast growing tumor that has been linked to more aggressive disease and worse overall outcome.[37,38] PD-L1 is highly expressed in tumor tissues compared to benign and indicates the tumor may be adapting to the immune system by inhibiting the native antitumor response.[39]

The assay developed in this study presents a multifaceted approach to evaluate the TME by detecting prostate-specific biomarkers (PSMA and p504s), immune biomarkers (CD8 and PD-L1), as well as a known prognostic biomarker (Ki-67) and an adjunctive diagnostic biomarker (basal cell cocktail).[40–42] We apply our 6-marker prostate assay to 2 distinct tissue microarrays (TMA) with 134 differentially graded PCa tissues. The prostate TMA tissues were then imaged on our hybrid high-order chromogenic multiplexing platform. The objective of this study was to evaluate if our chromogenic multiplex platform produced high-fidelity images that could be used to discover features that define the presence of cancer and to explore changes with tumor grade. To accomplish this goal, images of individual cancer biomarkers were quantified for protein abundance and expression levels were compared. Furthermore, we evaluated if our multiplexing platform could be used to evaluate spatial signatures, and after analysis we report several protein-to-protein distance relationships that are markedly closer in adenocarcinoma versus healthy prostate tissue. Interestingly, the majority of spatial descriptors that were found to be significantly different in healthy tissue were related to prostate-specific markers (p504s and PSMA).

Materials and methods

Background of analyzed tissue microarrays

Two different PCa TMAs were used in this prevalence study. The first TMA (Pantomics, Inc.) consisted of 102 cases of prostate tissue in which 7 cases were normal/benign and 95 cases had cancer. The age of the patients ranged between 34 and 90. Each core was labeled with disease type and cancer grade. Tissue cores had diameters of 1.5 mm. Out of 95 cancer cores, 94 cores were adenocarcinoma, and so only those tissues were analyzed. The second TMA (Novus Biologicals, LLC) consisted of 49 total prostate tissue cores (40 cancerous, 9 benign normal) from 40 patients. The age of the patients ranged between 44 and 75. Tissue cores from Novus Inc. had a diameter of 2 mm and were labeled with disease type, cancer grade, and Gleason score. Due to the larger diameter, this TMA was used for spatial analysis. Because both TMAs were labeled with cancer grade (I, II, or III), this feature was used for classification in this study. Tissues from each TMA were sectioned to a thickness of 4 μm. For both TMA vendors, all tissues were acquired in an anonymized fashion with informed consent.

Reagents and design of multiplex assay

A fully automated staining protocol was performed using a DISCOVERY ULTRA platform (Roche Tissue Diagnostics, Tucson, AZ). Antibodies were used against basal cell (cocktail of 34βE12 + p63, VMSI Cat# 790-4536), p504s (SP116, VMSI Cat# 790-6011), Ki-67 (30 − 9, VMSI Cat# 790-4286), PSMA (EP192, VMSI Cat # 760-6076), CD8 (SP57, VMSI Cat # 790-4460), and PD-L1 (SP263, VMSI Cat # 740-4907). Detection of these biomarkers was accomplished using the DISCOVERY RUO Purple kit (VMSI Cat# 760–229), and 5 other research chromogen substrates. The DISCOVERY Universal Procedure was used to create a protocol for the 6-plex IHC assay. All dyes were sourced from Roche Tissue Diagnostics. The antibody-chromogen assignments for the assay are listed in Table 1.

Staining began with tissue sections mounted on a glass slide that was warmed to 72 °C for 3, 8-min cycles to deparaffinize the tissue. The tissue was then prepped for staining by completing antigen retrieval, which consisted of using Cell Conditioning 1 (VMSI Cat# 950-124) and warming the slide to 100 °C for 64 min. Next, the primary antibody targeting the first biomarker in the panel was incubated following by a rinse in 1 × Reaction Buffer (VMSI Cat# 950-300). This was followed by incubating the anti-species antibody targeting the primary antibody (either anti-mouse HQ or anti-rabbit HQ) conjugated to anti-HQ HRP, washing with 1 × Reaction Buffer, incubating with tyramide chromogen or tyramide chromogenic precursor (DBCO) and hydrogen peroxide, and washing with 1 × Reaction Buffer. When using a precursor to the chromogen, a chromogenic dye was

Table 1
Overview of assay antibodies, clones, and chromogens used for the 6-plex prostate cancer assay.

Antibody	Clone	Dilution	Staining pattern	Dye	Color
Basal cell cocktail	34βE12 + p63	Pre-dilute	Cytosolic, Nuclear	N-Methyl Coumarin	Non-visible Near UV
CD8	SP57	Pre-dilute	Membranous	Rhodamine 110	Red-Pink
Ki-67	30-9	Pre-dilute	Nuclear	Rhodamine 800	Yellow
p504s	SP116	Pre-dilute	Cytosolic	Tamra	Purple
PD-L1	SP263	Pre-dilute	Cytosolic, Membranous, Nuclear (debated)	Cy7	Non-visible Near IR
PSMA	EP192	Pre-dilute	Cytosolic, Membranous	Coumarin 343	Yellow

added following the last 1× Reaction Buffer wash. Prior to staining the next detection stack in the assay, Cell Conditioning 2 (VMSI Cat# 950-123) was applied at 100 °C for 12 min and the slide was rinsed in 1× Reaction Buffer. This process was then repeated for all biomarkers in the multiplex assay. Unless the detection kits specified otherwise, multiplex IHC was performed at 37 °C. After IHC staining was complete, slides were counterstained by applying Hematoxylin II (VMSI Cat# 790-2208) for 4 min followed by applying Bluing (VMSI Cat# 760-2037) for 4 min. After counterstaining, the slide was rinsed in 1× Reaction Buffer and then dehydrated using a Sakura Tissue-tek Prisma (Sakura Finetek USA) with dehydration series through 3 × 100% ethanol, 1 min each, and 3× xylene, 1 min each at ambient temperature, and mounted in mounting media (Sakura Finetek USA) using an automated glass coverslipper (Tissue-Tek Glas g2, Sakura Finetek USA). The same staining protocol was used for both TMAs.

Additionally, standard H&E staining was performed on serial sections of each TMA so the tissue's morphology could be visualized. Fig. 1(a) and (b) present respective example fields of the H&E stain and pseudo-colored visualization of the multiplex assay in which significantly different tissue features can be observed.

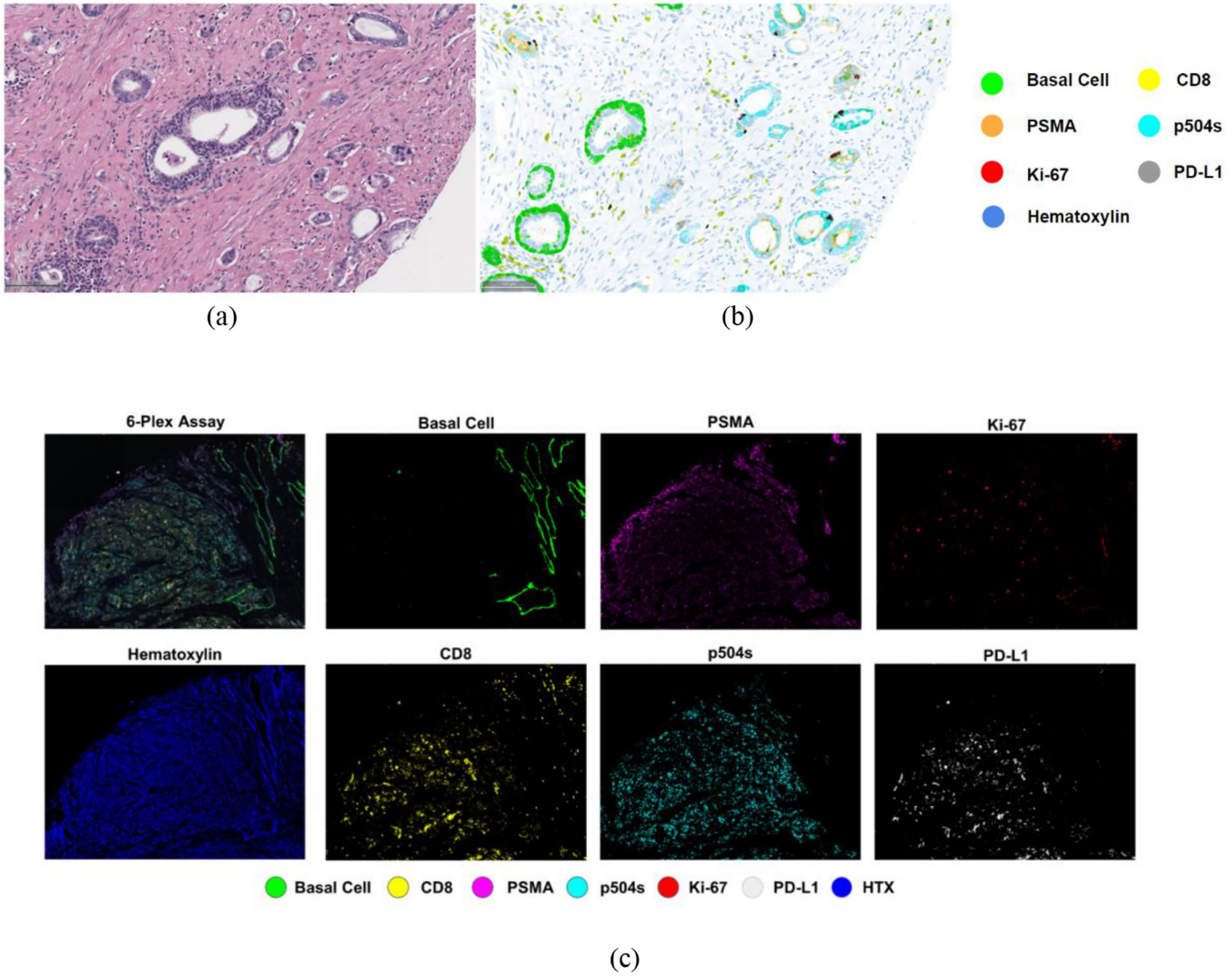

Fig. 1. Overview of 6-marker prostate multiplex assay. (a) Representative H&E image of adenocarcinoma prostate tissue. (b) Brightfield pseudo-colored visualization of 6-plex assay stained from serial section of (a). (c) Darkfield pseudo-colored visualization of 6-plex assay (top left) and images of the individual biomarker channels after spectral unmixing.

Image acquisition and spectral unmixing

Imaging of multiplex slides was performed by retrofitting an Olympus BX-63 microscope system (Olympus Corp.) with a pe-800 8-LED illumination system (CoolLED Limited) to permit spectroscopic imaging. Each channel of the pe-800 was paired with a custom-selected narrowband transmission optical filter to optimally pair each dye's absorption peak to an illumination channel. Multispectral image acquisition was acquired using an imaging macro written in the Cellsens software (Olympus Corp.). Initially, thumbnail images were acquired with a 4× objective (Olympus Corp., UPLXAPO4X). Subsequent high-resolution imaging was performed using a 20× objective (Olympus Corp., UPLXAPO20X). Once a multispectral image stack was acquired, the transmission image stack was converted to absorbance. Finally, spectral unmixing was performed to remove crosstalk using custom-developed software, to generate images of individual biomarkers, as displayed in Fig. 1(c). Performance of spectral unmixing was assessed analytically by calculating the signal-to-noise ratio (SNR) of each unmixed channel. For the biomarker-chromogens combinations used in this assay, the SNR was observed to be in the range of 50–100, meaning the average squared signal intensity was 50–100 times higher than the squared variation of the background signal. Ultimately, unmixing accuracy depends on many parameters including chromogens, biological targets, and the used assay. For subsequent image analysis and cell segmentation, individual mappings of biomarkers were used. Additional details regarding our imaging system are described in the literature.[23]

Cell segmentation and feature extraction

To perform feature extraction, analysis, and downstream processing, HALO (Indica Labs) and Python libraries were used. The HALO software suite was used to visualize images, extract features, and perform quantitative evaluation of tissues using a broad range of artificial intelligence (AI) and computer vision algorithms. In this study, Indica Lab's Highplex FL module was used to perform cell segmentation to extract cellular information and other features from the multiplex images. Example images of cell segmentation are presented in Fig. 2(a). Core- and cell-level features were extracted from the image using this module. In total, 26 core-level features (Table A.1) and 68 cell-level features (Table A.2) were extracted from the image. The Highplex FL module had multiple parameters which were fine-tuned to perform nuclear detection and cell quantification for different chromogens. Nuclear detection was carried out on the unmixed hematoxylin channel and chromogen threshold values were optimized for each

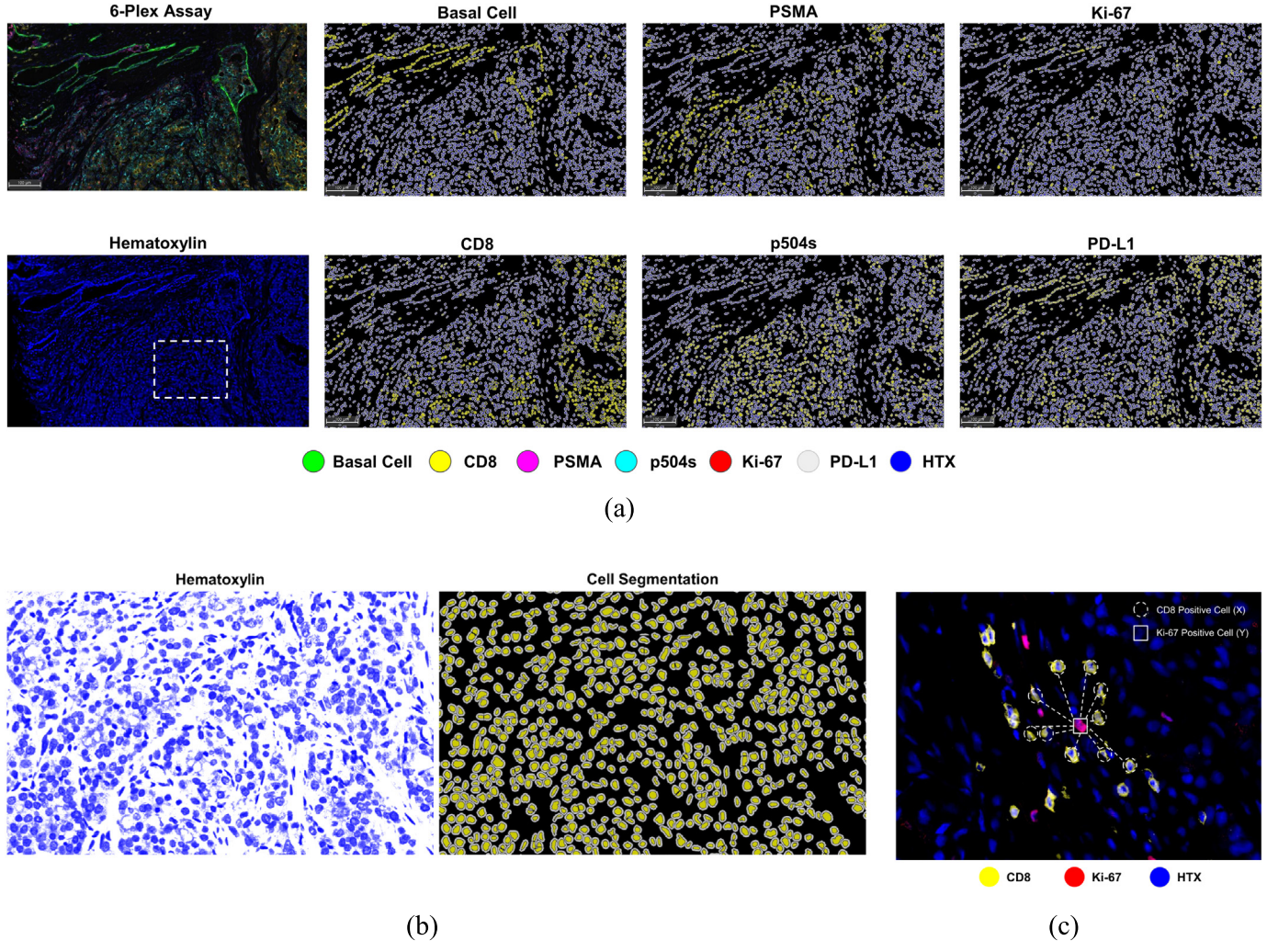

Fig. 2. Image segmentation and analysis. (a) Darkfield pseudo-colored visualization of 6-plex assay (left) and example images of cell segmentation performed for each biomarker in the assay (Basal cell, PSMA, Ki-67, CD8, p504s, and PD-L1) in adenocarcinoma PCa tissues using HALO software. Cells are either biomarker positive (yellow) or biomarker negative (blue). (b) Hematoxylin channel (left) and the associated cell segmentation image (right) from the HALO AI software module for the zoomed in dashed rectangle depicted in the Hematoxylin image of Fig. 2(a). (c) Visual representation of cell-to-cell distance calculation. The distances between an anchor cell positive for a given biomarker (Ki-67) and the 10 nearest cells positive for an interacting protein (CD8) are used to compute an average distance between the cell types.

channel. The prime parameters used for nuclear detection were nuclear segmentation type, nuclear contrast threshold, minimum nuclear intensity, and nuclear size. The "nuclear segmentation type" parameter was used in detecting and segmenting nuclei regions. A pre-trained AI model, within the HALO AI software package, performed the nuclear segmentation by utilizing contrast between the backdrop and the luminous nucleus. The amount of contrast necessary for nuclear detection was determined by the "nuclear threshold" parameter. The "minimum nuclear intensity" parameter ruled-out faintly dyed objects as nuclei and the "nuclear size" parameter was used to fine-tune nuclei detection by setting realistic limits for nuclei size. Example images of cell segmentation are displayed in Fig. 2(b). Cell segmentation parameters were chosen based on assessment by subject matter experts to optimize the performance of HALO AI's cell segmentation capabilities with our unmixed brightfield mappings of protein abundances. Different parameters were used to extract features from the TMAs (see Tables A.3 and A.4 for Pantomics TMA parameter specifications and Tables A.5 and A.6 for Novus TMA parameter specifications). For these experiments, the cell positivity values are considered in percentages, which is calculated by dividing the number of cells positive for a biomarker by the total number of cells and multiplied by 100.

A spatial biology analysis was performed on a subset of the PCa tissues by analyzing the intercellular distance between pairs of the 6 biomarkers in the multiplex assay. For this experiment, 18 cores of Novus TMA were considered, with 9 healthy and 9 adenocarcinoma tissues from matched patients. Intercellular distances of 377K cells were calculated using the Euclidean distance between each cell's X and Y coordinates. As described in Fig. 2(c), a cell(X) positive for a biomarker was chosen and a "window" of the 10 closest cells(Y), positive for a different biomarker were identified and the distance between each was calculated and averaged.[43] The same process was carried out for all permutations of the 6 biomarkers. Cells positive for both cancer antigens were excluded. Finally, the average distance for all biomarker combinations was calculated. Ultimately, spatial analysis was meant to capture cell-to-cell interactions and was used as a mechanism to extract meaningful relationships that describe tumor development and/or the immune response. A "window" of 10 cells was established based on previously published data from Schurch et al. in which they described a methodology to analyze patient tissue using cellular neighborhoods based on how cells are spatially arranged with respect to each other.[43] A window size of 10 cells represents an appropriate metric to assess the local density of individual cell types.

Python libraries were used for feature manipulation and for performing spatial analysis of the multiplex slide. For this experiment, 5 open-source Python libraries (Pandas, Matplotlib, Numpy, Umap, and scikit-learn) were used to analyze and visualize the features extracted from the images. Pandas is a powerful data analysis and manipulation tool used in analyzing textual and numerical data. Matplotlib is a data plotting library built on Numpy arrays that offers various charts and an easy to use data visualization tool. Uniform Manifold Approximation and Projection (UMAP) feature reduction was used to visualize features in a lower-dimensional space to help explore the complex dataset and identify clusters within the high-dimensional feature dataset. The lower dimensional core features were validated using k-means clustering algorithm.

Results

Profiling biomarker expression levels of adenocarcinoma in prostate cancer

We initially sought to explore the profile of PCa tissue by evaluating expression levels of each biomarker in the multiplex assay (Basal cell, PSMA, Ki-67, CD8, p504s, and PD-L1). To quantify the cell positivity percentage and correlate expression with cancer grade, 91 adenocarcinoma PCa cores of the Pantomics TMA were analyzed. Quantitative results are displayed in the box and whiskers plot in Fig. 3. PSMA and p504s were highly expressed compared to the other biomarkers. The average cell positivity percentage of the biomarkers were basal cell—2.49%, PSMA—15.93%, CD8—2.99%, Ki-67—6.76%, p504s—16.63%, PD-L1—4.87%. The highest average cell positivity percentage was observed in p504s followed by PSMA and CD8, respectively. From this dataset, one can observe that some markers have significantly more variability in expression levels (PSMA and p504s), whereas other biomarkers appear to have more consistent expression levels (Basal cell and CD8).

Next, biomarker expression levels were analyzed by cancer grade. The cumulative data was split into 3 subgroups: Grade I, II, and III for each biomarker. There were 14 Grade-I, 31 Grade-II, and 43 Grade-III adenocarcinoma cores. Fig. 4 presents whiskers and boxes of each individual biomarker's positivity percentage versus cancer grade for each tissue specimen. It's important to note that the samples lacked annotations to differentiate normal glands, tumor cells, or stromal cells. Integrating these distinctions could significantly enhance the granularity of our analysis. However, the visualization offers a clearer picture of how biomarker

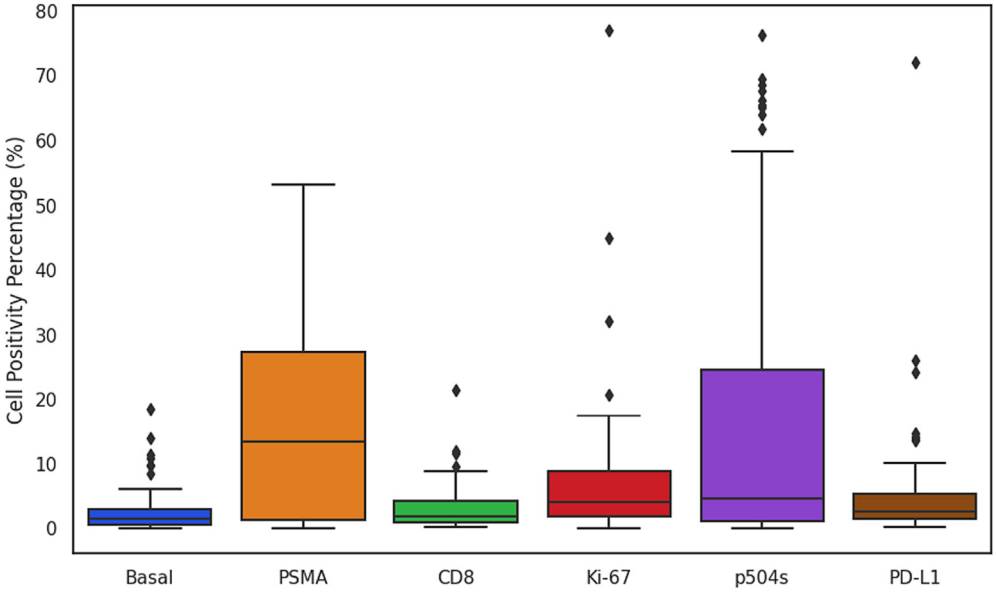

Fig. 3. Biomarker expression in adenocarcinoma PCa. Cell positivity percentage of basal cell, PSMA, Ki-67, CD8, p504s, and PD-L1. Gray bar represents the median, boxes represent the interquartile range, whiskers extend from 10% to 90%, and outliers are represented by diamonds (N = 91).

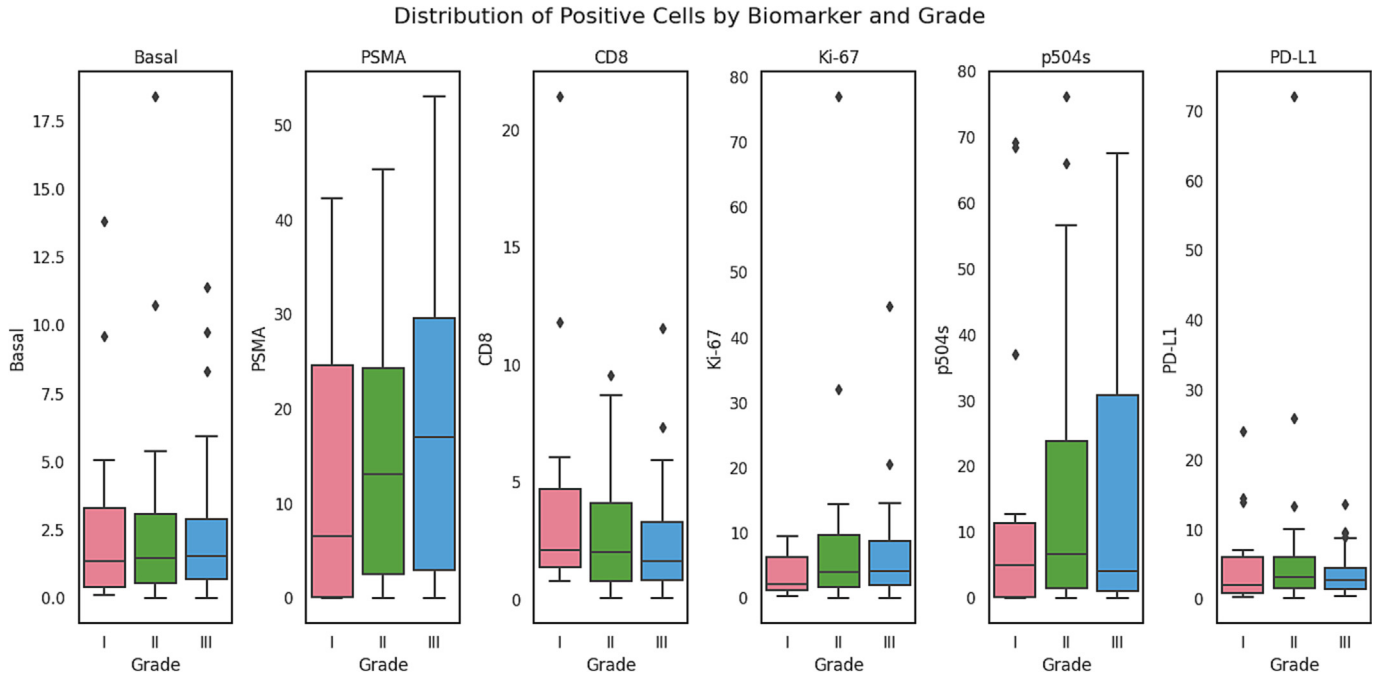

Fig. 4. Biomarker expression by grade in adenocarcinoma PCa. Biomarker positivity percentage of basal cell, PSMA, Ki-67, CD8, p504s, and PD-L1 in adenocarcinoma prostate cancer tissues (N = 88); subcategorized by cancer grades (I, II, and III). Gray bar represents the median, boxes represent the interquartile range, whiskers extend from 10% to 90%, and outliers are represented by diamonds.

positivity varies among different cancer grades. This technology thus enables proteomic analysis of cancer biomarker expression across disease states.

Profiling phenotypic descriptors of adenocarcinoma prostate cancer

A phenotypic analysis of biomarker expression was performed to survey which combinations of biomarker expression were correlated. The cell positivity values of adenocarcinoma cores from the Pantomics TMA were considered for correlation analysis. As displayed in Fig. 5, we see that basal cell expression is positively correlated with CD8 (0.55) as well as several other correlated biomarkers pairs with weaker correlated expressions. This indicates several phenotypes observed across the adenocarcinoma tissues that appear to have interdependencies with other cancer biomarkers and thus present potentially valuable targets for future research to understand the mechanism of the relationship. We also identify multiple biomarker combinations with independent expression levels as indicated with relatively low correlation coefficients (e.g., <0.2).

Profiling IHC signatures that differentiate healthy and cancerous tissue

In this section, the biomarker expression for adenocarcinoma and healthy tissue was compared. For this experiment, the biomarker cell positivity percentage of 18 total cores from the Novus TMA was considered. The dataset consisted of 9 adenocarcinoma PCa cores and 9 matched healthy cores. Although this is a small-scale underpowered study that is susceptible to sample variability, because the samples were matched, it presented a unique opportunity to directly compare diseased and healthy tissues. When comparing expression levels between healthy and cancerous tissue, substantial differences were detected and all biomarkers were found to have statistically significant differences. Complete results of the dataset are presented in Fig. 6. For 4 biomarkers (PSMA, CD8, p504s, and PD-L1), the cell positivity expression of adenocarcinoma tissues was higher compared to healthy tissues. Conversely, for basal cell and Ki-67, higher cell positivity was detected in healthy tissue compared to adenocarcinoma cores. For Ki-67, this is an unexpected result that may be an artifact of the low number of samples because Ki-67 is expressed in spreading cancerous tissues, although it has not been established as an independent prognostic marker.[37] Additionally, there was substantially more variability in several biomarker's expression in adenocarcinoma tissue when compared to a healthy baseline (Basal cell, PSMA, CD8, p504s, and PD-L1).

In the following section, we employed deep feature extraction and analysis algorithms to differentiate healthy and cancerous tissues using a rich set of features such as staining intensity and completeness, in addition to biomarker expression. Models were built to analyze tissues both at the macro-level (i.e., core-level) as well as at the scale of an individual cell (cell-level). For core-level analysis, 26 features were extracted and analyzed (Table A.1) and for cell-level analysis 64 features were extracted and analyzed (Table A.2). To differentiate healthy and adenocarcinoma cores using all of the extracted features, dimensionality reduction of core- and cellular-level features of the Novus TMA was employed. The 26 core-level features were labeled as healthy and adenocarcinoma. The data was reduced to 2 features using UMAP with optimized parameters (n_neighbors = 5, min_dist = 0.1, n_components = 2), selected based on parameter tuning experiments. K-means clustering (n_clusters = 2) to the extracted features for categorizing healthy and adenocarcinoma cores. The clustering achieved an ARI (Adjusted Rand Index) of 0.58, indicating substantial agreement with ground-truth labels and NMI (Normalized Mutual Information) of 0.59 supporting our effective separation of core types. Results are displayed in Fig. 7(a) with red data points representing adenocarcinoma cores and blue data points representing healthy cores. The 2 subgroups were well-differentiated into defined clusters. For cell-level clustering, 64 cell-level features were reduced to 2 features using the same UMAP algorithm. Results are displayed in Fig. 7(b) where each data point represents a single cell that is labeled based on cancer grade. Clusters of different cancer grades are labeled on the figure with delineated groups representing collections of Grade I, Grade II, and Grade II–III cells. Cell-level clusters were manually identified and marked using distinct colors; no clustering algorithms were employed in this process.

Spatial analysis of prostate cancer

In this section, the distance between cells expressing pairs of biomarkers was calculated and the values for adenocarcinoma and healthy cores were

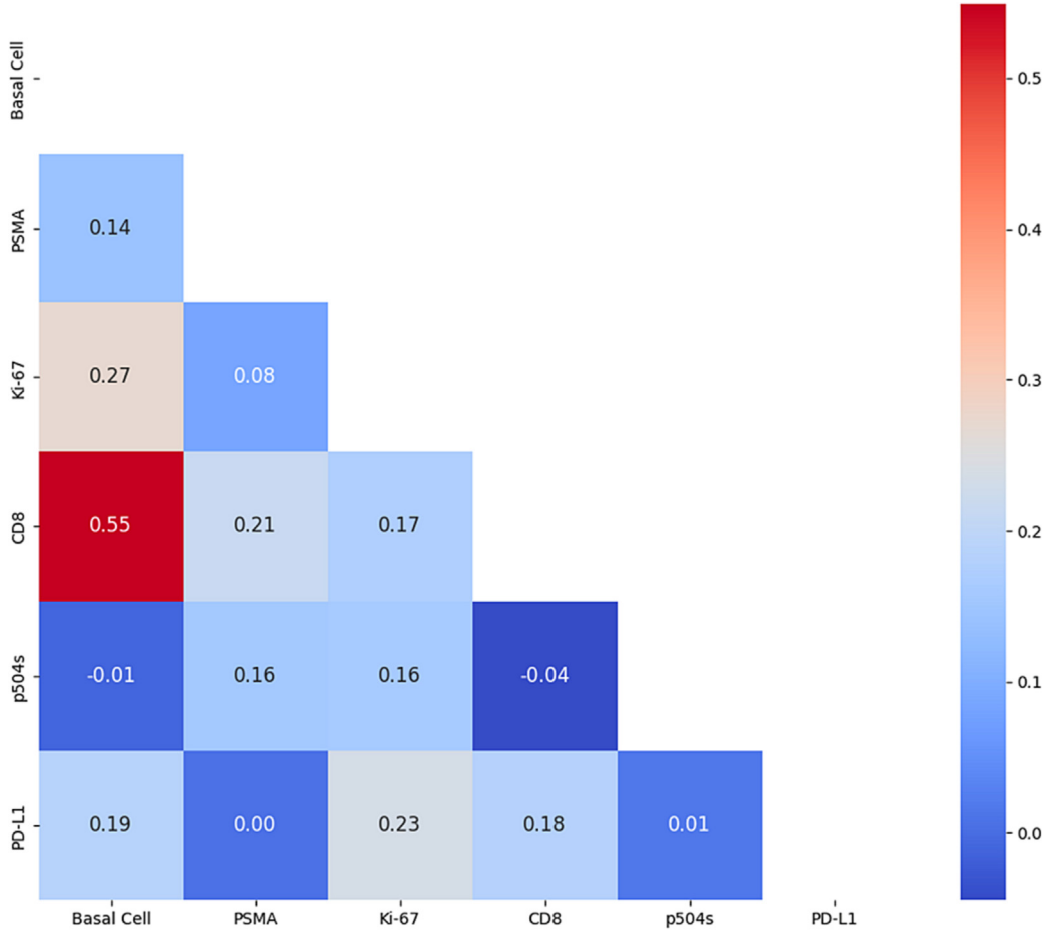

Fig. 5. Analysis of phenotypes expressed in adenocarcinoma PCa tissue. (a) Cellular-level correlation analysis of biomarkers (Basal cell, PSMA, Ki-67, CD8, p504s, and PD-L1) expressed in PCa tissue. The heatmap illustrates the strength and direction of correlations between these biomarkers providing insights into potential relationships among them.

compared. For this section, the larger Novus TMA cores were analyzed. The distances were ranked based on the highest difference and the top 13 values (<1.5×) were selected and included in Table 2. The ratio of distances between healthy and adenocarcinoma cores was calculated to generate a relative metric and is presented in the fifth column. The average closest distance between PD-L1 and p504s was found to be 3.52 times higher in healthy cores compared to adenocarcinoma cores. Similarly, the intercellular distance was at least 2× times higher in 4 other biomarker combinations (CD8 to p504s, Ki-67 to p504s, basal to p504s, and basal to Ki-67). This analysis reveals p504s positive cells tend to 2–3× closer to PD-L1, CD8, Ki-67, basal cell, and PSMA positive cells in cancerous adenocarcinoma tissue versus healthy tissue. This observation is potentially supported in the literature because p504s is upregulated in cancer tissue which would present more opportunities for p504s positive cells to be in close proximity to other cell phenotypes.[34]

Discussion

As our understanding of the tumor microenvironment grows, there is an increased need for solutions that can detect multiple analytes within the context of the tissue to better understand mechanisms that are driving tumor growth. Furthermore, with a larger number of detected analytes, drawing insights from the data becomes increasingly difficult for pathologists which drives the need for digital analysis support. Ultimately, multiplexed assays used in conjunction with digital algorithms will be critical to match patients with a therapy that is optimally suited to be effective against their disease and will preserve precious tissue to facilitate testing with orthogonal methods, such as sequencing. Multiple multiplexing solutions have been developed recently that hold promise to meet this need such as mass spectroscopy,[44–46] spatial transcriptomics,[47–49] and immunoflourescent-based IHC staining.[19,50] Although all of these techniques hold great promise as research tools to study cancer characteristics, each faces significant hurdles to clinical implementation such as cost, throughput, standardization, integration into clinical workflow, reimbursement, and acceptance by worldwide laboratories.[51,52]

In this work, we present a hybrid multiplexing platform that has many of the benefits of clinically implemented brightfield microscopy but has been augmented with a novel spectroscopic imaging system as well as narrowband chromogenic dyes that enable high-order multiplexing with brightfield imaging. Because brightfield multiplex imaging is not typically associated with digital analysis, there is little work exploring the suitability of brightfield multiplex images with digital pathology algorithms.[20] We address this need by exploring the characteristic profile of PCa samples that were imaged and analyzed with our chromogenic multiplexing platform after developing a 6 marker panel that targets prostate-specific biomarkers (PSMA and p504s), the immune profile (CD8 and PD-L1), as well as a known prognostic marker (Ki-67) and diagnostic marker (basal cell cocktail). Overall, 143 different PCa tissues were analyzed. We report that the cell positivity percentages showed several patterns across different cancer grades. Dozens of features from each tissue were extracted and UMAP dimensionality reduction was used to distinguish adenocarcinoma and healthy cores. The reduced-dimensional features were fed into the k-means clustering algorithm, successfully clustering the cores with an accuracy of 89%. Additionally, a spatial analysis was performed to explore the intercellular distance between cells expressing different biomarkers. Multiple biomarker combinations were found to have different spatial

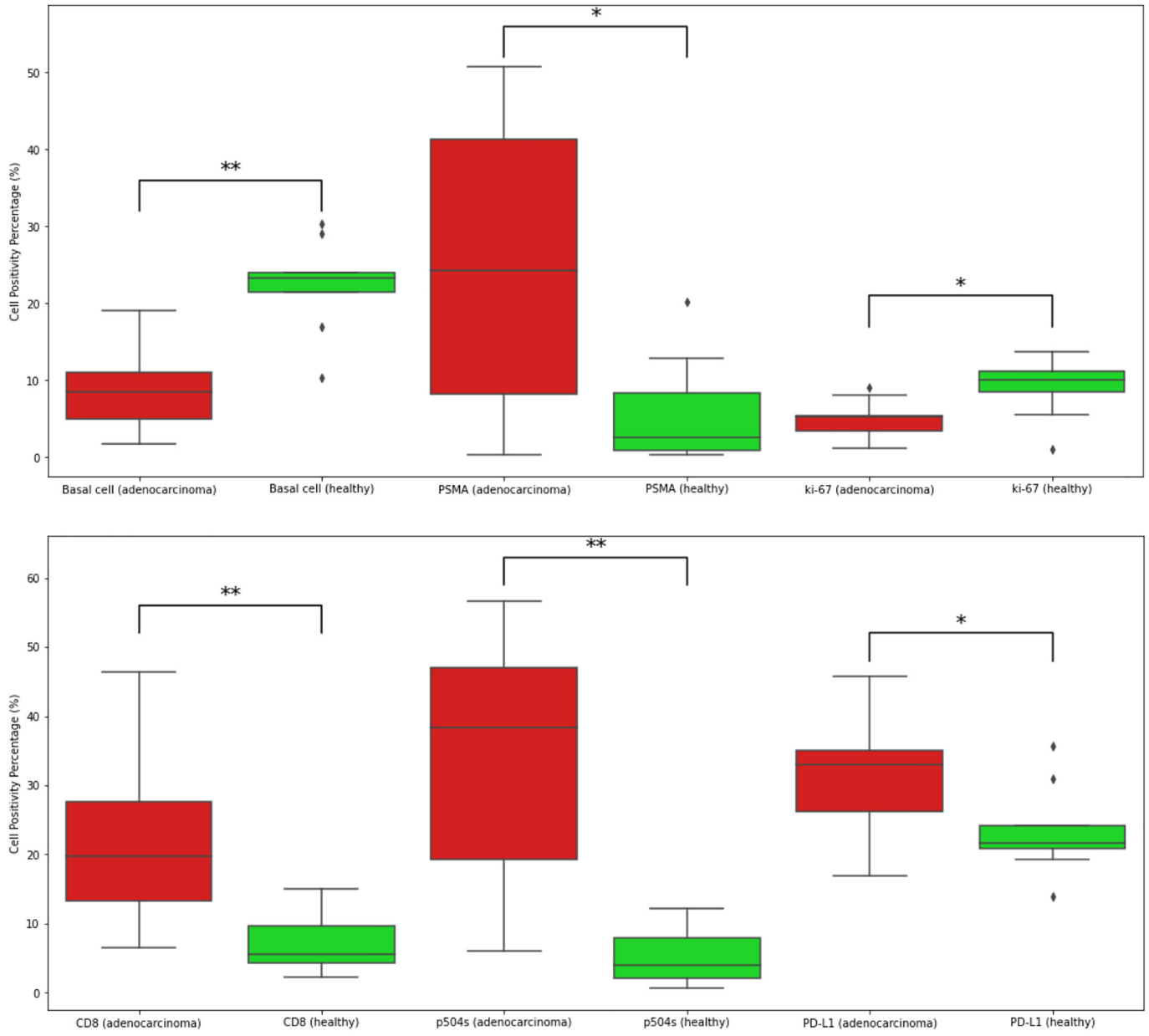

Fig. 6. Comparison of biomarker expression between healthy and adenocarcinoma PCa tissue. Cell positivity percentage of adenocarcinoma PCa tissues (N = 9, red) and matched healthy tissues (N = 9, green). *P*-value annotation legend: ns: 5.00e-02 <*P*<=1.00e+00, *: 1.00e-02<*P*<=5.00e-02, **: 1.00e-03<*P*<=1.00e-02, ***: 1.00e-04<*P*<=1.00e-03, ****: *P*<=1.00e-04. Gray bar represents the median, boxes represent the interquartile range, whiskers extend to 10%–90%, and outliers are represented by diamonds.

organizations including PD-L1 and p504s which were 3.52 times further apart in healthy tissues relative to adenocarcinoma cores.

We thus present data that our multiplexing platform can be combined with digital analysis tools to create a novel diagnostic platform that can be used for next generation diagnostic assays. One potential use of this diagnostic system would be to better understand which patients will respond to immunotherapy. Immunotherapy is one area where a deep understanding of the tumor's molecular signature is critical. Immunotherapy harnesses the power of the adaptive immune system by equipping the patient's own immune system with the ability to recognize and attack antigen presenting cancer cells. These novel therapeutic treatments have been shown to produce durable responses in patients with several distinct cancer types such as melanoma and non-small cell lung cancer and have revolutionized the field of oncotherapy providing benefit to countless patients.[53] However, complete response rates to immune checkpoint inhibitors remain at ~20%, which indicates that more advanced diagnostic assays are needed to better predict which subsets of patients will respond to immunotherapy-based treatments.[54,55] Thus, combining our next-gen diagnostic platform with nex-gen therapies presents an attractive option for future development. Additionally, this multiplexing platform could be an enabling technology to push digital pathology, machine learning, and spatial biology algorithms into clinical practice. We note that cell segmentation and feature extraction were performed using HALO's Highplex FL module, which is a software suite developed for use with mIF images. Thus, we demonstrate that our brightfield multiplex images are compatible with algorithms designed for fluorescent images.

There are potential weaknesses with this study and the technology platform. For instance, the work presented here is from a relatively small cohort of samples which potentially biases the results (see Ki-67 finding). In the future, applying the system to a larger cohort of data would be valuable to yield more reliable results. Although not a limitation of brightfield multiplexing but rather our current implementation, it is worth noting

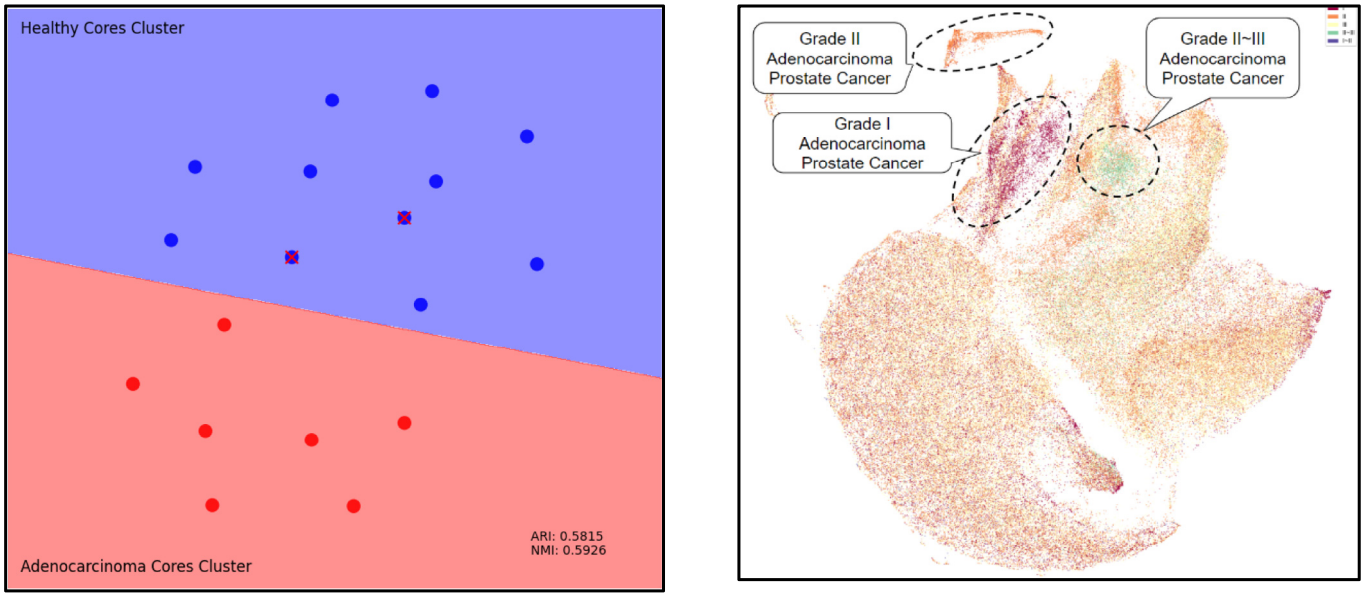

Fig. 7. Differentiating healthy and adenocarcinoma prostate tissue with dimensionality reduction. (a) UMAP (Uniform Manifold Approximation and Projection) visualization of core-level features extracted from adenocarcinoma PCa (N = 18) tissue samples. The data has been clustered into 2 distinct groups using the k-means clustering algorithm, misclassified samples are marked with X symbol. (b) UMAP representation of cell-level features of 50 adenocarcinoma PCa tissue samples. A total of 104 875 cells were analyzed.

that the analysis performed in this experiment were based on tissue-level classification of cancer grade and not on annotated regions of the sample's subcompartments (tumor, stroma, and benign glands). This capability will be incorporated into future work and will enable even deeper characterization of the tumor-immune microenvironment such as tissue compartment specific assessment (e.g., PD-L1 expression in tumor cells) as well as investigation of additional spatial features (e.g., distance to tumor boundary). With this in mind, and considering the relatively low number of tissue samples in the study, the reader should be cautious about pathologic interpretations from this study until validated by additional studies with more rigorous biological controls in place. Another potential gap in the system is to characterize and optimize how accurately a biomarker's dynamic range can be detected by the system. Although we expect the dynamic range to be larger than that of traditional light microscopy, future work will be needed to evaluate the limits of the dynamic range in more detail. Finally, the multiplexing imaging platform presented here is a technology demonstration and does not represent a commercial-grade product that could be easily used for larger studies. A more mature hardware platform would be needed to facilitate larger translational studies or eventual clinical adoption.

Table 2
Table comparing the average distances between pairs of biomarkers.

Biomarker combination		Adenocarcinoma (μm)	Healthy (μm)	Healthy/ Adenocarcinoma
Reference cell (X)	Neighbor cells (Y)			
PD-L1	p504s	131.0	461.0	3.52
CD8	p504s	116.6	372.1	3.2
Ki-67	p504s	124.2	348.2	2.81
Basal	p504s	140.3	337.3	2.41
Basal	Ki-67	345.2	754.7	2.19
PSMA	p504s	136.1	268.2	1.98
PD-L1	PSMA	243.7	479.9	1.97
CD8	PSMA	254.7	465.4	1.83
Ki-67	PSMA	214.0	362.6	1.7
p504s	PSMA	290.2	474.1	1.64
PD-L1	CD8	147.0	235.8	1.61
Basal	CD8	96.6	148.6	1.54
Ki-67	CD8	86.9	131.8	1.52

Conclusions

In this work, the characteristic profile of PCa tissues were analyzed with a novel hybrid multiplexing platform, demonstrating that our chromogenic multiplexing system is a powerful tool that can be used to investigate the TME by extracting features that may be used to understand cancer growth and to ultimately deliver the most accurate diagnostic results. This work details that chromogenic high-order multiplexing is compatible with AI-based analytical tools and digital pathology algorithms which can help to automate the analysis of large amounts of data and identify complex patterns that may not be apparent to the human eye. Chromogenic imaging boasts several advantages such as overall robustness, expedited workflow, established trust, and customer familiarity in the clinical setting. Thus, by combining chromogenic high-order multiplexing with advanced analytical tools, researchers can enjoy a hybrid technology that can facilitate digital multianalyte readouts in a potentially clinically applicable form factor. This technology platform could enable the rapid translation of spatial biology-based research into clinical practice, leading to improved diagnostic accuracy and better treatment outcomes for patients. Overall, the presented brightfield multiplexing system combines the clinical applicability and widespread acceptance of brightfield assays with the rising diagnostic power of high-order multiplexing and digital pathology algorithms and is well-suited for translational studies and potentially eventual clinical adoption.

Funding

Funding for this study was provided by Roche Diagnostics Solutions.

Declaration of Competing Interest

RR, RB, MW, BK, and DB were employed at Roche Diagnostics Solutions during this study. RB, MW, BK, and DB are holders of equity and/or stock

options Roche Diagnostics Solutions. RB, BK, and DB have patents related to this technology although they receive no royalties on them.

Acknowledgments

We would like to acknowledge Benjamin Stevens for sharing his expertise in using the HALO software and performing image analysis.

Appendix A. Supplementary data

Supplementary data to this article can be found online at https://doi.org/10.1016/j.jpi.2023.100352.

References

1. Jaffer S, Bleiweiss IJ. Beyond hematoxylin and eosin—the role of immunohistochemistry in surgical pathology. Cancer Invest 2004;22(3):445–465.
2. Chan JKC. The wonderful colors of the hematoxylin–eosin stain in diagnostic surgical pathology. Int J Surg Pathol 2014;22(1):12–32.
3. Rosai J. Why microscopy will remain a cornerstone of surgical pathology. Lab Invest 2007;87(5):403–408.
4. Koelzer VH, Grobholz R, Zlobec I, Janowczyk A, Swiss Digital Pathology Consortium (SDiPath). Update on the current opinion, status and future development of digital pathology in Switzerland in light of COVID-19. J Clin Pathol 2021;75(10):687–689.
5. Taube JM, Akturk G, Angelo M, et al. The Society for Immunotherapy of Cancer statement on best practices for multiplex immunohistochemistry (IHC) and immunofluorescence (IF) staining and validation. J Immunother Cancer [Internet] 2020;8(1). Available from: https://doi.org/10.1136/jitc-2019-000155.
6. Hofman P, Badoual C, Henderson F, et al. Multiplexed immunohistochemistry for molecular and immune profiling in lung cancer—just about ready for prime-time? Cancers 2019;11(3):283.
7. Yeong J, Fox BA, Sater HA, Rodriguez-Canales JA, McKee TD. *Multiplex Immunohistochemistry/Immunofluorescence Technique: The Potential and Promise for Clinical Application*. Frontiers Media SA. 2022.
8. Ng HHM, Lee RY, Goh S, et al. Immunohistochemical scoring of CD38 in the tumor microenvironment predicts responsiveness to anti-PD-1/PD-L1 immunotherapy in hepatocellular carcinoma. J Immunother Cancer [Internet] 2020;8(2). Available from: https://doi.org/10.1136/jitc-2020-000987.
9. Tsujikawa T, Kumar S, Borkar RN, et al. Quantitative multiplex immunohistochemistry reveals myeloid-inflamed tumor-immune complexity associated with poor prognosis. Cell Rep 2017;19(1):203–217.
10. Ilié M, Beaulande M, Ben Hadj S, et al. Chromogenic multiplex immunohistochemistry reveals modulation of the immune microenvironment associated with survival in elderly patients with lung adenocarcinoma. Cancers [Internet] 2018;10(9). Available from: https://doi.org/10.3390/cancers10090326.
11. Lu S, Stein JE, Rimm DL, et al. Comparison of biomarker modalities for predicting response to PD-1/PD-L1 checkpoint blockade: a systematic review and meta-analysis. JAMA Oncol 2019;5(8):1195–1204.
12. Banik G, Betts CB, Liudahl SM, et al. High-dimensional multiplexed immunohistochemical characterization of immune contexture in human cancers. Methods Enzymol 2020;635:1-20.
13. Johnson DB, Bordeaux J, Kim JY, et al. Quantitative spatial profiling of PD-1/PD-L1 interaction and HLA-DR/IDO-1 predicts improved outcomes of anti–PD-1 therapies in metastatic melanoma. Clin Cancer Res 2018;24(21):5250–5260.
14. Kwak JT, Hewitt SM, Kajdacsy-Balla AA, Sinha S, Bhargava R. Automated prostate tissue referencing for cancer detection and diagnosis. BMC Bioinformatics 2016;17(1):227.
15. Tsujikawa T, Mitsuda J, Ogi H, et al. Prognostic significance of spatial immune profiles in human solid cancers. Cancer Sci 2020;111(10):3426–3434.
16. Zwanenburg ES, Wisselink DD, Klaver CEL, et al. The measured distance between tumor cells and the peritoneal surface predicts the risk of peritoneal metastases and offers an objective means to differentiate between pT3 and pT4a colon cancer. Mod Pathol 2022;35(12):1991–2001.
17. Nagl S, Haas M, Lahmer G, et al. Cell-to-cell distances between tumor-infiltrating inflammatory cells have the potential to distinguish functionally active from suppressed inflammatory cells. Oncoimmunology 2016;5(5), e1127494.
18. Feichtenbeiner A, Haas M, Büttner M, Grabenbauer GG, Fietkau R, Distel LV. Critical role of spatial interaction between $CD8^+$ and $Foxp3^+$ cells in human gastric cancer: the distance matters. Cancer Immunol Immunother 2014;63(2):111–119.
19. Tan WCC, Nerurkar SN, Cai HY, et al. Overview of multiplex immunohistochemistry/immunofluorescence techniques in the era of cancer immunotherapy. Cancer Commun 2020;40(4):135–153.
20. Ugolini F, Pasqualini E, Simi S, Baroni G, Massi D. Bright-field multiplex immunohistochemistry assay for tumor microenvironment evaluation in melanoma tissues. Cancers [Internet] 2022;14(15). Available from: https://doi.org/10.3390/cancers14153682.
21. Shakya R, Nguyen TH, Waterhouse N, Khanna R. Immune contexture analysis in immuno-oncology: applications and challenges of multiplex fluorescent immunohistochemistry. Clin Transl Immunology 2020;9(10), e1183.
22. Day WA, Lefever MR, Ochs RL, et al. Covalently deposited dyes: a new chromogen paradigm that facilitates analysis of multiple biomarkers in situ. Lab Invest 2017;97(1):104–113.
23. Morrison LE, Lefever MR, Behman LJ, et al. Brightfield multiplex immunohistochemistry with multispectral imaging. Lab Invest 2020;100(8):1124–1136.
24. Morrison LE, Lefever MR, Lewis HN, Kapadia MJ, Bauer DR. Conventional histological and cytological staining with simultaneous immunohistochemistry enabled by invisible chromogens. Lab Invest 2022;102(5):545–553.
25. Pivetta E, Capuano A, Scanziani E, et al. Multiplex staining depicts the immune infiltrate in colitis-induced colon cancer model. Sci Rep 2019;9(1):12645.
26. Fassler DJ, Abousamra S, Gupta R, et al. Deep learning-based image analysis methods for brightfield-acquired multiplex immunohistochemistry images. Diagn Pathol 2020;15(1):100.
27. Bonkhoff H. Role of the basal cells in premalignant changes of the human prostate: a stem cell concept for the development of prostate cancer. Eur Urol 1996;30(2):201–205.
28. Signoretti S, Waltregny D, Dilks J, et al. p63 is a prostate basal cell marker and is required for prostate development. Am J Pathol 2000;157(6):1769–1775.
29. Raskov H, Orhan A, Christensen JP, Gögenur I. Cytotoxic CD8+ T cells in cancer and cancer immunotherapy. Br J Cancer 2021;124(2):359–367.
30. Yang Y, Attwood K, Bshara W, et al. High intratumoral CD8+ T-cell infiltration is associated with improved survival in prostate cancer patients undergoing radical prostatectomy. Prostate 2021;81(1):20–28.
31. Bostwick DG, Pacelli A, Blute M, Roche P, Murphy GP. Prostate specific membrane antigen expression in prostatic intraepithelial neoplasia and adenocarcinoma: a study of 184 cases. Cancer 1998;82(11):2256–2261.
32. Kinoshita Y, Kuratsukuri K, Landas S, et al. Expression of prostate-specific membrane antigen in normal and malignant human tissues. World J Surg 2006;30(4):628–636.
33. Wright Jr GL, Haley C, Beckett ML, Schellhammer PF. Expression of prostate-specific membrane antigen in normal, benign, and malignant prostate tissues. Urol Oncol 1995;1(1):18–28.
34. Jiang Z, Woda BA, Rock KL, et al. P504S: a new molecular marker for the detection of prostate carcinoma. Am J Surg Pathol 2001;25(11):1397–1404.
35. Rüschoff JH, Stratton S, Roberts E, et al. A novel 5x multiplex immunohistochemical staining reveals PSMA as a helpful marker in prostate cancer with low p504s expression. Pathol Res Pract 2021;228, 153667.
36. Fantony JJ, Howard LE, Csizmadi I, et al. Is Ki67 prognostic for aggressive prostate cancer? A multicenter real-world study. Biomark Med 2018;12(7):727–736.
37. Verma R, Gupta V, Singh J, et al. Significance of p53 and ki-67 expression in prostate cancer. Urol Ann 2015;7(4):488–493.
38. Richardsen E, Andersen S, Al-Saad S, et al. Evaluation of the proliferation marker Ki-67 in a large prostatectomy cohort. PLoS One 2017;12(11), e0186852.
39. Palicelli A, Bonacini M, Croci S, et al. What do we have to know about PD-L1 expression in prostate cancer? A systematic literature review. Part 1: Focus on immunohistochemical results with discussion of pre-analytical and interpretation variables. Cells [Internet] 2021;10(11). Available from: https://doi.org/10.3390/cells10113166.
40. Zellweger T, Günther S, Zlobec I, et al. Tumour growth fraction measured by immunohistochemical staining of Ki67 is an independent prognostic factor in preoperative prostate biopsies with small-volume or low-grade prostate cancer. Int J Cancer 2009;124(9):2116–2123.
41. Berney DM, Gopalan A, Kudahetti S, et al. Ki-67 and outcome in clinically localised prostate cancer: analysis of conservatively treated prostate cancer patients from the Trans-Atlantic Prostate Group study. Br J Cancer 2009;100(6):888–893.
42. Kristiansen G. Markers of clinical utility in the differential diagnosis and prognosis of prostate cancer. Mod Pathol 2018;31(S1):S143–S155.
43. Schürch CM, Bhate SS, Barlow GL, et al. Coordinated cellular neighborhoods orchestrate antitumoral immunity at the colorectal cancer invasive front. Cell 2020;182(5):1341-1359.e19.
44. Risom T, Chang P, Rost S, Ziai J. Mass spectrometry-based tissue imaging of the tumor microenvironment. Methods Mol Biol 2023;2660:171–185.
45. Ptacek J, Locke D, Finck R, et al. Multiplexed ion beam imaging (MIBI) for characterization of the tumor microenvironment across tumor types. Lab Invest 2020;100(8):1111–1123.
46. Levenson RM, Borowsky AD, Angelo M. Immunohistochemistry and mass spectrometry for highly multiplexed cellular molecular imaging. Lab Invest 2015;95(4):397–405.
47. Zhang L, Chen D, Song D, et al. Clinical and translational values of spatial transcriptomics. Signal Transduct Target Ther 2022;7(1):111.
48. Yoosuf N, Navarro JF, Salmén F, Ståhl PL, Daub CO. Identification and transfer of spatial transcriptomics signatures for cancer diagnosis. Breast Cancer Res 2020;22(1):6.
49. Maniatis S, Petrescu J, Phatnani H. Spatially resolved transcriptomics and its applications in cancer. Curr Opin Genet Dev 2021;66:70–77.
50. Hernandez S, Rojas F, Laberiano C, Lazcano R, Wistuba I, Parra ER. Multiplex immunofluorescence tyramide signal amplification for immune cell profiling of paraffin-embedded tumor tissues. Front Mol Biosci 2021;8, 667067.
51. Heaney LM, Jones DJ, Suzuki T. Mass spectrometry in medicine: a technology for the future? Future Sci OA 2017;3(3).FSO213.
52. Harms PW, Frankel TL, Moutafi M, et al. Multiplex immunohistochemistry and immunofluorescence: a practical update for pathologists. Mod Pathol 2023;36(7), 100197.
53. Esfahani K, Roudaia L, Buhlaiga N, Del Rincon SV, Papneja N, Miller Jr WH. A review of cancer immunotherapy: from the past, to the present, to the future. Curr Oncol 2020;27(suppl 2):S87–S97.
54. Meng J, Lu X, Zhou Y, et al. Tumor immune microenvironment-based classifications of bladder cancer for enhancing the response rate of immunotherapy. Mol Ther Oncolytics 2021;20:410–421.
55. Sharma P, Hu-Lieskovan S, Wargo JA, Ribas A. Primary, adaptive, and acquired resistance to cancer immunotherapy. Cell 2017;168(4):707–723.